RSC Advances

This article can be cited before page numbers have been issued, to do this please use: H. Ghafuri, F. Mohammadi, R. Rahimi and E. mohammadiyan, *RSC Adv.*, 2016, DOI: 10.1039/C6RA17712C.

View Article Online
DOI: 10.1039/C6RA17712C

RSC Advances

Dynamic Article Links►

Cite this: DOI: 10.1039/c0xx00000x

www.rsc.org/xxxxxx

ARTICLE TYPE

Synthesis and charactrization of a new magnetic nanocomposite with metalloporphyrin (Co-TPyP) and sulfated tin dioxide (Fe_3O_4@SnO_2/SO_4^{2-}), and investigation of its photocatalytic effects on degradation of Rhodamine B

Hossein Ghafuri*[a], Fatemeh Mohammadi[a], Rahmatallah Rahimi[a] and Esmaeel Mohammadiyan[a]

[a] *Catalysts and Organic Synthesis Research Laboratory, Department of Chemistry, Iran University of Science and Technology, Tehran 16846-13114, Iran*

Received (in XXX, XXX) XthXXXXXXXXX 20XX, Accepted Xth XXXXXXXXX 20XX
DOI: 10.1039/b000000x

Abstract: For synthesis of (Fe_3O_4@SnO_2/SO_4^{2-}), after preparation of magnetic nanoparticle Fe_3O_4 (MNP), tin dioxide was supported on MNP, and it was sulphated by Ammonium sulfate. To improve the photocatalyitic activity of this magnetic nanocatalyst, after synthesis of 5, 10, 15, 20-Tetra (4-pyridyl) porphyrin and its cobalt metalloporphyrin, (Co-TPyP) was stabilized on Fe_3O_4@SnO_2/SO_4^{2-}.The structure and morphology were characterized by XRD, EDX, FT-IR, SEM and FE-SEM. The X-ray diffraction studies show tetragonal SnO_2 and orthorhombic structure of Fe_3O_4. The Fe_3O_4@SnO_2/SO_4^{2-} as an acidic heterogeneous nanocatalyst with excellent magnetic properties can be easily separated from the reaction an external magnetic field. The photocatalytic activity was investigated by photodegradation of Rhodamine B (RhB) in aqueous solution under visible light irradiation. The simplicity workup processes, low cost catalyst and high efficiency in degradation of RhB are from outstanding advantages of this procedure.

Introduction

The screening and synthesis of new nanostructure metal oxides are from intresting field in research institutes. Due to their rich surface chemical/electronic properties, they are sensitive to light and have suitable photocatalyitic activites. Recently have been published considerable reports to finding the low cost and high-yield procedures to synthesis of nanostructured oxides, and to improve their especial applications such as removal toxic organic pollutants and in clean energy devices[1]. From among them, metal oxides have attracted great attention due to their high theoretical specific capacity[2]. Iron oxides such as Fe_3O_4 are one kind of transition metal oxide, which in particular has a high electrical conductivity than most other metal oxides[3]. Superparamagnetic Fe_3O_4 nanoparticles are widely used for information storage, biomolecule imaging, sensing, separation, etc. SnO_2 is from other important nanoparticles which act as a nanocrystalline and is used as chemical sensor for many molecules[4]. It is also employed as photoelectrode in solar cells. Due to its unique photoelectric properties, chemical stability, and nontoxicity, it also has been considered as photo catalyst [5] in some chemical reactions.

SnO_2, also is employed as n-type semiconductor, possesses interesting optical and optoelectronic properties[6-10]. SnO_2 has been widely studied for electronic and photoelectronic devices[11-13]. However many binary sulfides can cause secondary pollution due to the photo-erosion problem[14], which limits their further applications. In addition, SnO_2 is an excellent semiconductor with high stability and acid/alkali resistance[15]. In spite of wide usages, the difficulty of recovery process of nanoparticles is from other limitations which prevent to adoption of this technology by industries. Magnetic separation of the photocatalyst powder is a possible solution, and Fe_3O_4@SnO_2 nanocomposite serves the purpose which the elegant combinations of the porous SnO_2 shell with the conductive core Fe_3O_4, interestingly[16]. Also, sulfated tin oxide (SO_4^{2-}/SnO_2) has been used in some catalytic oxidation process[17]. Traditionally, catalysts such as H_2SO_4, H_3PO_4, and $AlCl_3$ used in chemical processes exhibit good activity, but many of these catalysts are environmentally harmful. Regarding to above mentioned limitations, there has been great interest to development of non-toxicity solid acid catalysts. Supported solid acids, especially sulfated metal oxides, are suitable replacements for the conventional homogeneous counterparts due to their several advantages such as strong acidity, relative easy separation, environmental friendliness, and high activity in some organic reactions even at low temperatures[18]. From the other side, porphyrins and its derivatives are from high usage pieces with outstanding properties in some organic reactions [19-22]. The properties of porphyrin like its coordination chemistry, emission capabilities, optical and electronic abilities, and conjugated

View Article Online
DOI: 10.1039/C6RA17712C

arrays have been considered along the years. Porphyrins play the key roles in a numerous synthetic multicomponent reactions at simulating the operation of the photosynthetic reaction centres [23]. In aspect of pollutants removal procedures, porphyrins have well absorptions and can be used for reduce pollutants of phenols (with photo oxidation of them). Tetrakis porphyrin and its metal derivatives also are from strong sensitizer for this action[24]. Metalloporphyrins, which have unique biological, chemical, physical, and catalytic functionalities, represent a remarkable class of molecule-based solids[25,26] Because of their distinctive catalytic activities[27], the inclusion of metalloporphyrins in porous coordination networks has gained intense attention, and some of them have shown very interesting catalytic properties in heterogeneous reactions[25,28]. Due to increasing the uses of chemical pollutants in various industries, the entering of organic contaminants in drinking water causes to serious problems in our lives. For this reason, the purification of contaminated water [29], has been found great importance recently. Biological purification of these pollutants for the low efficiency is not appropriate to this aim. In the resent researches photocatalytic process was used to removal of some environmental pollutants [30-34]. There is special attention to removal or degradation of many contaminants like Rhodamine B by metalloporphyrins absorbents. In our former published we showed the efficiency of porphyrin derivatives in degradation of pollutants [30]. In this work, after preparation of a new magnetic nanocatalyst Fe3O4@SnO2/SO_4^{2-} as an strong heterogeneous acid, its nanocomposite with cobalt metalloporphyrin (Co-TPyP) was synthesized and the photocatalytic activity was investigated by degradation of aqueous solution of Rhodamine B as an important environmental pollutant under visible light irradiation. Our researches have shown that this nanocomposite (Fe_3O_4@SnO_2/SO_4^{2-}-Co-TPyP) can improve the photocatalytic activity of porphyrin and metaloporphyrin and has higher efficiency than bare Fe_3O_4@SnO_2 in degradation of Rhodamine B.

Experimental

Materials and methods

All of the chemicals used in this work were obtained from Merck and used without further purification. Infrared (IR) spectra were carried out on a Shimadzu FT-IR-8400S spectrophotometer using a KBr pellet. The DRS spectra were prepared via a Shimadzu MPC-2200 spectrophotometer. The UV-Vis spectra were recorded on a Shimadzu (mini 1240 double beam) spectrophotometer in the wavelength range of 400-600 nm. The particle morphologies were observed by field emission scanning electron microscopy (FE-SEM) at 26 kV (KYKY-EM3200). The X-ray diffraction measurement was performed using graphite monochromatic copper radiation (Cu Kα) at 40 kV, 40 mA over the 2θ range of 10–80◦.

Synthesis of 5,10,15,20-Tetra(4-pyridyl)porphyrin (TPyP)

Propionic acid (100 ml) and acetic acid (1.5 ml) were mixed in a three-neck flask under nitrogen atmosphere and in reflux condition. Simultaneously, 4-pyridine carbaldehyde (1.5 ml) dropwise was added to the mixture. Then distilled pyrrole (1.105 ml) was added slowly to the mixture under nitrogen gas atmosphere and reflux was continued for 1h. IR (KBr): ν_{max} = 3419(N-H), 2850-2900(CH, Ar), 1591(C=N, pyrrol), 1000-1360 (C-N) cm^{-1}. UV-Vis: λ_{max} = 418nm^{-1} (Soret band), 514, 550, 590, 648nm^{-1} (Q bands).

Synthesis of complex 5,10,15,20-Tetra(4-pyridyl)porphyrin cobalt(II) [Co-TPyP] by (TPyP).

0.01 g of TPyP and 0.1 g $CoCl_2.6H_2O$ was dissolved in DMF. The mixture was refluxed for 3.5 h. The mixture was cooled to room temperature and after filtration the crude product was obtained. The product was washed with distilled water and dried in an oven at 60. IR (KBr): ν_{max} = 2985, 1608, 1431, 1153, 1014, 740, 518cm^{-1}. UV-Vis: λ_{max} = 440nm^{-1} (Soret band), 554, 612nm^{-1} (Q bands).

Preparation of the magnetic Fe_3O_4 nanoparticles (M*NPs*)

Ferric acid and ferrous salts were employed as precursors for the synthesis of Fe_3O_4 nanoparticles. Briefly, $FeCl_3.6H_2O$ (12.2 g, 0.04 mol) and $FeCl_2.4H_2O$ (4.7 g, 0.02 mol) were dissolved in 100 ml distilled water under vigorous stirring. After 10 minutes, the solution was heated at 50°C under nitrogen atmosphere. Consequently, the ammonium hydroxide solution (25%) was added dropwise to the reaction mixture to maintain the reaction pH about 9. Afterward, the reaction mixture was cooled at room temperature and black precipitate which was separated by external magnet from the reaction mixture, repeatedly washed with de-ionized water for several times to remove the remaining impurities. At the final step nanoparticles was dried at 60°C in vacuum.

Synthesis of Fe_3O_4@SnO_2/SO_4^{2-}

Initially 0.3g Fe_3O_4 NPs were dissolved in 50 ml EtOH:H_2O (1:1) and $SnCl_2$ (2.93 g) was added to to the mixture. To adjust the PH of mixture between 7-8, aqueous ammonia (10%) was added dropwise under vigorous stirring condition. The precipitate was filtered, thoroughly washed with distilled water; the absence of chloride ion was confirmed by $AgNO_3$ test. Subsequently the obtained solid was dipped in $(NH_4)_2SO_4$ (6 $mol.L^{-1}$) aqueous solution at room temperature for 24 h. Then the solid was filtered, dried without washing overnight at 100°C and calcination was done under nitrogen atmosphere at 500°C for 4 h**.**

Optimization of sulfation condition of Fe_3O_4@SnO_2/SO_4^{2-}

For imobilization of SO_4^{2-} on the surface of Fe_3O_4@SnO_2 in the first step, we should sulfated Fe_3O_4@SnO_2. To sulfate Fe_3O_4@SnO_2 (Fe/Sn 4:1) nanoparticles, different concentration of $(NH_4)_2SO_4$ solution including 4M, 5M and 6M was used. Charactrization of products by FT-IR spectra had shown that the best result was obtained with 6M soultion. (including two sharp and strong peak, one at 1205cm^{-1} for vibrational strenght of S=O and other at 1400cm^{-1} for asymmetric vibrational strenght).

In second step, to achieve the best magnetic property, calcination of synthesized Fe_3O_4@SnO_2/SO_4^{2-} was investigated in air and under nitrogen atmosphere. In the air atmosphere, nanoparticle of Fe_3O_4 was changed to Fe_2O_3 which had not shown magnetic properties. (Because of the presence of O_2 with oxidation process). Calcination of Fe_3O_4@SnO_2/SO_4^{2-} under nitrogen atmosphere with different molar ratio of Fe/Sn was carried out. The results were shown that the Fe/Sn 1:2 ratio has the best magnetic property among the three ratio of Fe/Sn: 1:1, 1:2 and 1:3.

Titration of Fe_3O_4@SnO_2/SO_4^{2-} and determination of acidity

To measurement of the acidity of synthesized catalyst back titration was used. 0.5 g of Fe_3O_4@SnO_2/SO_4^{2-} with 0.5 g NaCl was dissolved in 35 mL distillated water. 10 mL NaOH (0.1M) was added to the mixture and stirred for 24h. phenolphetalein indicator dropwisely was added to the mixture until the color of

View Article Online
DOI: 10.1039/C6RA17712C

mixture was changed to purple. For titration of the solution, HCl (0.1M) was added to the mixture until equivalence point was obtained. Finally, the calculations have shown that the pH of our synthesized catalyst is equal to 1.55.

Preparation of Fe_3O_4@SnO_2/SO_4^{2-}-Co-TPyP.

To synthesis of Fe_3O_4@ SnO_2/SO_4^{2-}-Co-TPyP, (0.01 g) synthesized Co-TPyP and (0.1 g) Fe_3O_4@SnO_2/SO_4^{2-} nanoparticle was dispersed in 10 mL ethanol. The mixture was stirred for 24 h at room temperature. After completion the reaction the solid product was obtained and collected by filtration. The obtained product was washed with ethanol and dried in vacuum.

Photocatalytic degradation

For degradation of 40 mL aqueous solution of Rhodamine B, 40 mg of Fe_3O_4@SnO_2/SO_4^{2-}-Co-TPyP photocatalyst was used. Before irradiation, the suspension was stirred in the dark condition for 30 min. Then, in the presence of irradiation, samples were taken every 30 min in 4 h. The photocatalytic degradation of the samples was recorded by UV-Vis spectrum.

Result and discussion

Catalyst characterization

FT-IR spectra analysis

The FT-IR spectra of Fe_3O_4 (a), Fe_3O_4@SnO_2(b), Fe_3O_4@SnO_2/SO_4^{2-}(c) in KBr were recorded in the range of 400-4000 cm^{-1}. As shown in Fig. 1 a broad peak about 3400 cm^{-1} was observed which is attributed to σ O-H stretching mode of water that adsorbed from air on the surface of catalyst. Hydrogen bonding causes the broadness of this peak. A peak about 1630 cm^{-1} attributed to δ O-H bending mode of water associated with the sulfate group. A strong band assigned to the stretching vibration of S=O observed about 1130 cm^{-1} and a middle peak at approximately 1400 cm^{-1} observed in the spectra assigned to asymmetric of covalent σ S=O bond. The peak at around 650cm^{-1} attributed to Sn-O [35,36] bond and the vibration peak of Fe-O [37] bond at about 500cm^{-1}. The IR spectra of Fe_3O_4@SnO_2/SO_4^{2-}-TPyP and Fe_3O_4@SnO_2/SO_4^{2-}-Co-TPyP are shown in Fig. 2. The N-H bending vibration bond appears about 3444 cm^{-1} that approves pyrrole ring. C-H stretching of Ar group vibrations appears at 2900 cm^{-1}. Moreover disappearance of N-H in Fig. 2 vibration around 3444 cm^{-1} in this spectrum shows that the related metalloporphyrins were also quantitatively prepared [38] .

Also, in (Fig 1.c) a broad and strong peak is appeared at 3200 cm^{-1} which can be ascribed to OH in sulphate groups. In two former spectra this peak is appeared very weaker probably due to absorption of surface water.

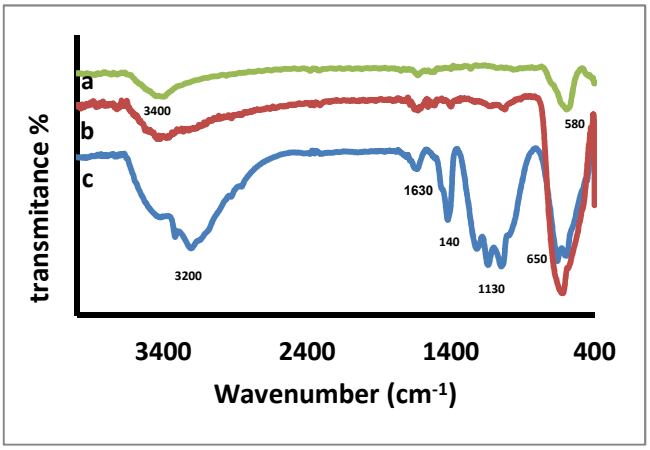

Fig 1. FT-IR spectrum of Fe_3O_4 (a) Fe_3O_4@SnO_2(b) Fe_3O_4@SnO_2/SO_4^{2-} (c)

Comparative FT-IR spectra of porphyrin (a) and metalloporphyrin (b) in Fig. 2 clearly shown that after the synthesis of metalloporphyrin the N-H peak (3444 cm^{-1}) has been omitted. Difference of these two compounds is only in addition of cobalt ion in porphyrin cavity and the omission of this peak at 3400 cm^{-1} is clear evidence to confirm that the synthesis successfully is done.

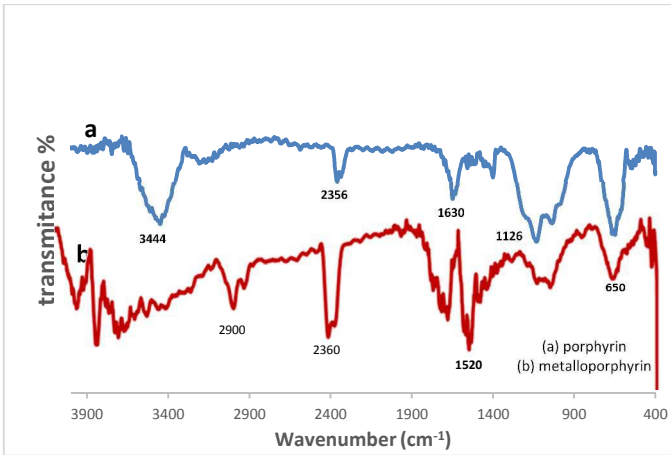

Fig 2. FT-IR spectra of porphyrin (a) and metalloporphyrin (b) on the catalyst

SEM study

By studying FE-SEM images, morphology, particle size and surface uniformity can be identified. FE-SEM images of Fe_3O_4@SnO_2, Fe_3O_4@SnO_2/SO_4^{2-} and Fe_3O_4@SnO_2/SO_4^{2-}-Co-TPyP nanoparticles are shown in Fig. 4. Regarding to this image and size distribution diagram (Fig 3), the highest aboundance of size distribution was seen in the range of 40- 45nm. According to the FE-SEM images, nanoparticles are spherical and have a good uniformity. As can be seen, porphyrin has not been created any change in the monoclinic morphology of the nanoparticles.

View Article Online
DOI: 10.1039/C6RA17712C

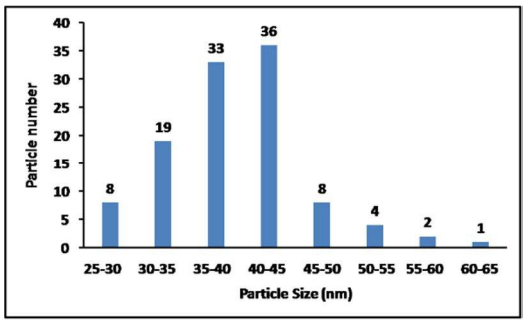

Fig 3. The graphs of size distribution $Fe_3O_4@SnO_2/SO_4^{2-}$ by using Excel software

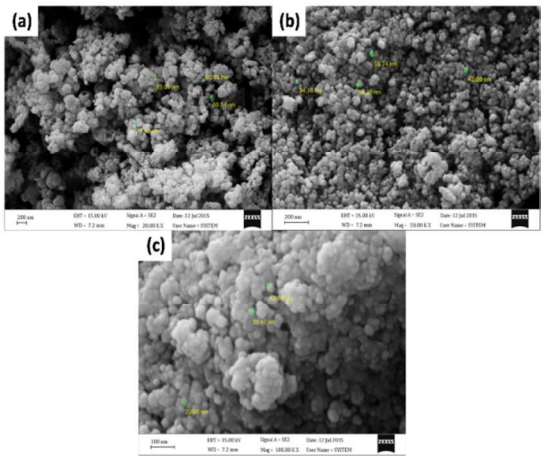

Fig 4. FE-SEM images of nanoparticles of a) $Fe_3O_4@SnO_2$, b) $Fe_3O_4@SnO_2/SO_4^{2-}$ and c) $Fe_3O_4@SnO_2/SO_4^{2-}$- Co-TPyP

XRD study

Fig. 5 shows the XRD patterns of the prepared Fe_3O_4, SnO_2, $Fe_3O_4@SnO_2/SO_4^{2-}$ and $Fe_3O_4@SnO_2/SO_4^{2-}$- Co-TPyP. As can be seen in Fig. 5, six characteristic peaks of Fe_3O_4 (2θ= 30.1, 35.4, 43.0, 53.5, 57.0 and 62.5) are observed. Also, considerable similarity of Fe3O4 peak with $Fe_3O_4@SnO_2/SO_4^{2-}$ (XRD pattern of $Fe_3O_4@SnO_2/SO_4^{2-}$) shows that the peak positions of Fe_3O_4 are unchanged during the production of $Fe_3O_4@SnO_2/SO_4^{2-}$ and $Fe_3O_4@SnO_2/SO_4^{2-}$-Co-TPyP. This clearly indicates that the crystalline structure of the magnetite is essentially maintained. In the SnO_2 spectrums three characteristic peaks are observed include (2θ= 26.6, 33.8, and 51.78) which the tetragonal structure is confirmed.

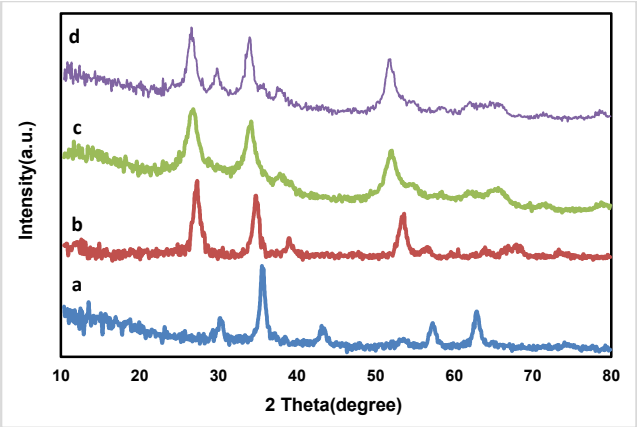

Fig 5. The X-ray diffraction patterns of a) Fe_3O_4 ,b)SnO_2, c) $Fe_3O_4@SnO_2/SO_4^{2-}$ and d) $Fe_3O_4@SnO_2/SO_4^{2-}$-Co-TPyP

DRS analysis

According to DRS spectra in Fig. 6 (a and b), we found that there is no absorption above 400 nm for $Fe_3O_4@SnO_2$ and $Fe_3O_4@SnO_2/SO_4^{2-}$, while in Fig. 6 c the supported catalyst shows the characteristic peaks of soret band and makes apparent that porphyrin successfully established on the $Fe_3O_4@SnO_2/SO_4^{2-}$ nanoparticles surface with maintaining the porphyrin structure.

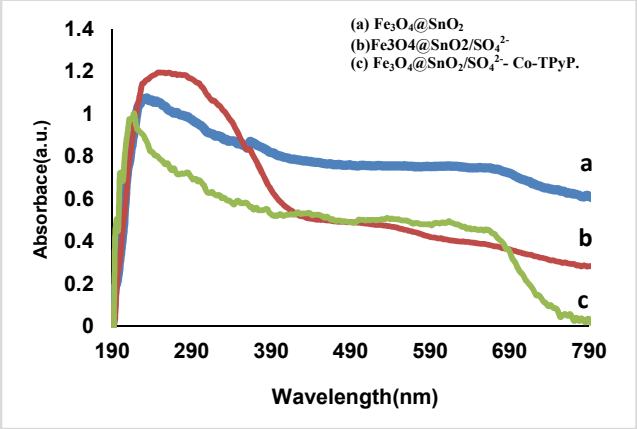

Fig 6. DRS spectra of a) $Fe_3O_4@SnO_2$ (b)Fe3O4@SnO2/SO_4^{2-} (c) $Fe_3O_4@SnO_2/SO_4^{2-}$- Co-TPyP.

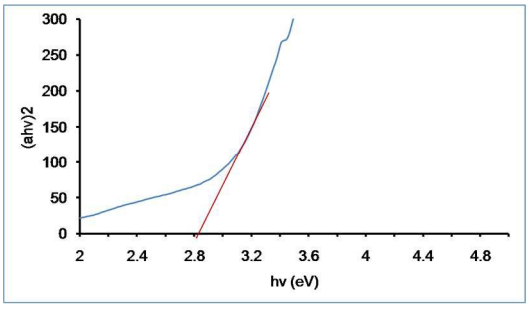

Fig 7. Drawn curve to estimating of gap band of $Fe_3O_4@SnO_2/SO_4^{2-}$.

View Article Online
DOI: 10.1039/C6RA17712C

The gap band of $Fe_3O_4@SnO_2/SO_4^{2-}$ is estimated by Tauc equation, DRS spectra and calculation curve in Fig 7. The result has shown that the gap bond is 2.9 ev.

VSM spectrum

In the results of the analysis of a vibrating sample magnetometer spectrum, which given in the Fig. 8, it is estimated that magnetic nanoparticles was reduced their super magnetic behavior after composition with porphyrin. Fig. 8 obviously has shown that the saturation magnetization of nanocomposite $Fe_3O_4@SnO_2/SO_4^{2-}$-Co-TPyP has been decreased than $Fe_3O_4@SnO_2$. This decrase is due to coating on the surface of $Fe_3O_4@SnO_2$ by $SO_4^{2-}$and Co-TPyP.

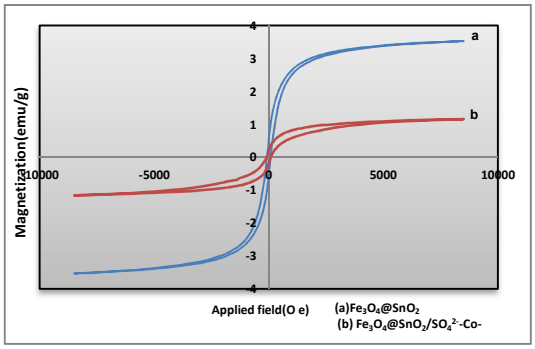

Fig 8. VSM Spectra of $Fe_3O_4@SnO_2$ and $Fe_3O_4@SnO_2/SO_4^{2-}$-Co-TPyP

EDX analysis

Fig. 9 presents the energy-dispersive X-ray (EDX) spectra of prepared nanocomposites. This spectrum confirms the presence of iron and tin in the prepared composites. The EDX spectra also show a lack of impurity in the prepared nanocomposites.

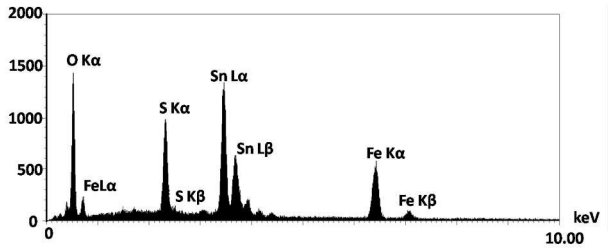

Fig 9. EDX spectra of prepared composites $Fe_3O_4@SnO_2/SO_4^{2-}$

Investigation of the photodynamic degradation of Rhodamine B (RHB)

To evaluate the efficiency of synthesized photocatalyst the photocatalytic degradation of Rhodamin B (RhB) in concentration of 10 ppm in the presence of light (lamp LED 5W) was done to evaluate the synthesized photocatalyst. The results after four hours of exposure by UV-Vis spectra were summerized on absorption spectrum (Fig11). As can be seen in Fig. 11 different functional groups have different degradation on the substrate nanoparticles. Table 1 has shown the results of degradation of Rhodamine B by nanoparticles. Degradation presentages of RhB by each of synthesized nanoparticles and their composite were compared. SnO_2, Fe_3O_4, $Fe_3O_4@SnO_2$ and $Fe_3O_4@SnO_2/SO_4^{2-}$ were investigated respectively. In the $Fe_3O_4@$ SnO_2/SO_4^{2-}—TPyP, the TPyP were attached by of π bond, ionic and van der Waals interaction on the surface of the magnetic nanoparticles. With this expansion resonance in the phenyl rings of TPyP, electron transfer can be done better and caused to increasing in degradation of Rhodamine B. Also the existence metals in the center of tetra pyrrole rings of porphyrin increased more photocatalysis activity compared to the free porphyrin. Therefore metalloporphyrins with further electron transfer enhances catalyst activity and the degradation percentage of RhB.

Table 1. Result of degradation percentage

Entry	Catalyst	Degradation (%)
1	SnO_2	25
2	Fe_3O_4	35
3	$Fe_3O_4@$ SnO_2	50
4	$Fe_3O_4@$ SnO_2/SO_4^{2-}	73
5	$Fe_3O_4@$ SnO_2/SO_4^{2-}-TPyP	85
6	$Fe_3O_4@$ SnO_2/SO_4^{2-}-Co-TPyP	99

Photocatalysis process

The degradation mechanism of RhB with diverse photocatalytic process has been reported[39,40]. The Fig 10 has shown the plausible mechanism of this research.
It is generally believed that the photocatalytic activity of SnO_2 is only in the range of UV light due to a broad Eg of about 5 ev.

Regading to broad range of Eg for SnO_2 (5 ev), the photocatalytic activity can been only in the range of UV light. So, the coated on the surface of Fe_3O_4, with a low band gap about 1.6 ev or lower can successfully absorb sunlight. porphyrin can improved the photocatalytic performance of $Fe_3O_4@SnO_2/SO_4^{2-}$ magnetic nanoparticles. It is obvious in Fig 10, under the visible light irradiation, photocatalytic process of $Fe_3O_4@SnO_2/SO_4^{2-}$-Porphyrin is sensitized and with a photon transition, positive and negative charges is created by electron converted from the ground state to the excited state of porphyrin. The produced electron more than transferred to the porphyrin surface also injected into the conduction band of SnO_2, owing to The CB level of SnO_2 is near the CB of porphyrin. Also, the electrons in the valence band (VB) of SnO_2 are excited to its conduction band (CB) under irradiation and so generate an equal amount of holes in its VB. The photogenerated holes transfer from the VB of SnO_2 to the VB of porphyrin. Therefore, it can be decrease the probability of electron–hole recombination. When the density of electrons was increased in the CB of SnO_2, these

View Article Online
DOI: 10.1039/C6RA17712C

electrons can react with molecular oxygen to produce O^{o}_2. Correspondingly, the OH^{o} was generated through an oxidative process when the holes on the porphyrin surface were attracted electrons from water and hydroxyl ions. Finally the produced radicals cause to degradation of Rhodamine B [40-42]. (Equation 1-6).

$[Fe_3O_4@SnO_2/SO_4^{2-}\text{-Co-TPyP}] + h\upsilon \rightarrow [Fe_3O_4@SnO_2/SO_4^{2-}\text{-Co-TPyP}]^*$ **(1)**

$[Fe_3O_4@SnO_2/SO_4^{2-}\text{-Co-TPyP}]^* \rightarrow Fe_3O_4@SnO_2/SO_4^{2-}\ [\text{Co-TPyP}]^+ + e^-_{CB}$ **(2)**

$e^-_{CB} + O_2 \rightarrow O_2^{\circ-}$ **(3)**

$h^+_{VB} + OH^- \rightarrow OH^{\circ}$ **(4)**

$O_2^{\circ-} + RhB \rightarrow$ Oxidation products **(5)**

$OH^{\circ} + RhB \rightarrow$ Oxidation products **(6)**

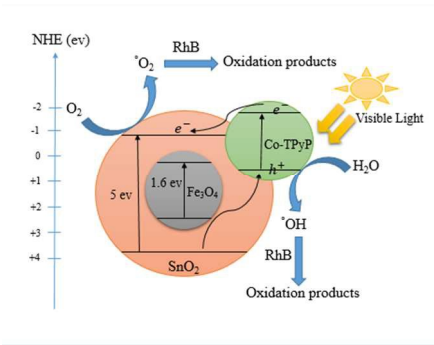

Fig 10. The plausible mechanism of degradation of RhB.

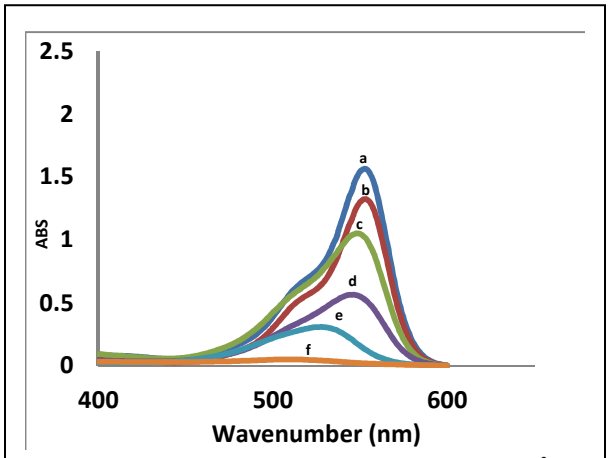

(a) SnO_2, (b) Fe_3O_4, (c) $Fe_3O_4@SnO_2$, (d) $Fe_3O_4@SnO_2/SO_4^{2}$ (e) $Fe_3O_4@SnO_2/SO_4^{2-}$-TPyP, (f) $Fe_3O_4@SnO_2/SO_4^{2-}$- Co-TPyP

Fig 11. Absorption spectrum of distruction of RHB(10 ml,10 ppm) after 4h irradiation in the presence of 10 mg catalyst in room temperature

Kinetic diagram

The equation: $D = [C_0 - C/C_0] \times 100$ was used to obtain the degradation of Photocatalyst. The synthetic graphs were drawn based on the reaction rate which was shown in Fig 12.

C_0 is the initial uptake of contaminants in the absence of photocatalysis and C is the adsorption after the exposure time. In the first samples were taken for 30 minutes in the dark without light, and that the equilibrium adsorption - desorption is achieved and when the sample was exposed to the light, the photocatalitic degradation is completed. Fig.12, is indicated that the degradation of Rhodamine B in the absence of catalyst is small amount in percentage.

The results of table.1 and Fig.12 have shown that the degradation of pollutant with $Fe_3O_4@\ SnO_2/SO_4^{2-}$catalyst is 73%. When it is attached to porphyrin (TpyP) the photocatalytic degradation increased to 85% and this shown the effective role of porphyrin to improve the degradation efficiency. Also, the percentage of degradation was increased to 99% when its nanocomposite with cobalt metalloporphyrin (Co-TPyP) was used. These results have shown that the entering of metal in the cavity of porphyrin cause to enhancement of electron transfer process and it increase degradation efficiency of metalloporphyrin nanocomposite

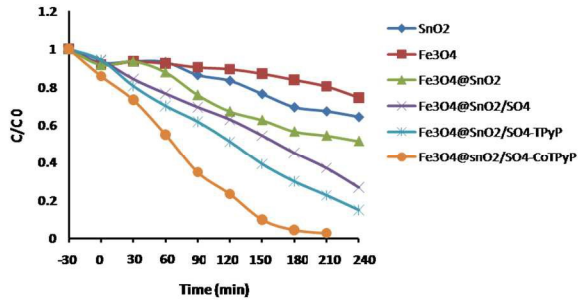

Fig 12. Kinetic diagram of RHB (40 ml, 10 ppm) degradation under vs irradiation times in the presence of 40 mg catalyst

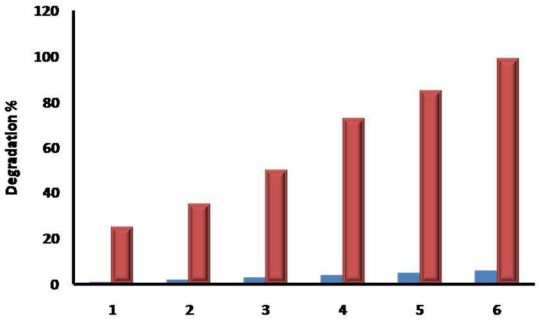

Fig 13. Degradation percentage of RHB (10 ppm) using of 10 mg 1) SnO_2 2)Fe_3O_4 3)$Fe_3O_4@SnO_2$ 4)$Fe_3O_4@SnO_2/SO_4^{2}$ 5)$Fe_3O_4@SnO_2/SO_4^{2-}$-TPyP 6) $Fe_3O_4@SnO_2/SO_4^{2-}$- Co-TPyP

Conclusions

After preparation of magnetic nanoparticle (MNP) Fe_3O_4, tin dioxide was supported on this MNP and was sulphated by $(NH_4)_2SO_4$. The charactization of synthesized magnetic nanocatalyst $Fe_3O_4@SnO_2/SO_4^{2-}$ was done by FT-IR, DRS, SEM, FE-SEM, XRD, EDX and VSM techniques. In order to improvement of the photocatalyitic activity, its nanocomposite cobalt metalloporphyrin (Co-TPyP) was synthesized and then

View Article Online
DOI: 10.1039/C6RA17712C

stabilized on Fe_3O_4@SnO_2/SO_4^{2-}. The photocatalytic activity was investigated by photodegradation of Rhodamine B in aqueous solution under visible light irradiation. The results had shown that the Fe_3O_4@SnO_2/SO_4^{2-}-Co-TPyP has excellent efficiency in degradation of RhB. The easy separation of catalyst due to excellent magnetic properties and simplicity workup process are from other remarkable advantages of this procedure.

Acknowledgments

The authors gratefully acknowledge the partial support from the Research Council of the Iran University of Science and Technology.

Notes and references

Catalysts and Organic Synthesis Research Laboratory, Department of Chemistry, Iran University of Science and Technology, Tehran 16846-13114, Iran 16846_13114, Fax: 982177491204; Tel: 982177240516-7, E-mail: ghafuri@iust.ac.ir.

1. X. Duan, G. Wang, H. Wang, Y. Wang, C. Shen and W. Cai, *CrystEngComm*, 2010, **12**, 2821-2825.
2. X. Sun, W. Si, X. Liu, J. Deng, L. Xi, L. Liu, C. Yan and O. G. Schmidt, *Nano Energy*, 2014, **9**, 168-175.
3. R. Li, X. Ren, F. Zhang, C. Du and J. Liu, *Chemical Communications*, 2012, **48**, 5010-5012.
4. E. Comini, C. Baratto, G. Faglia, M. Ferroni, A. Vomiero and G. Sberveglieri, *Progress in Materials Science*, 2009, **54**, 1-67.
5. Y. Han, X. Wu, Y. Ma, L. Gong, F. Qu and H. Fan, *CrystEngComm*, 2011, **13**, 3506-3510.
6. Y. Han, X. Wu, G. Shen, B. Dierre, L. Gong, F. Qu, Y. Bando, T. Sekiguchi, F. Filippo and D. Golberg, *The Journal of Physical Chemistry C*, 2010, **114**, 8235-8240.
7. F. Song, H. Su, J. Han, J. Xu and D. Zhang, *Sensors and Actuators B: Chemical*, 2010, **145**, 39-45.
8. Z. Li, H. Wang, P. Liu, B. Zhao and Y. Zhang, *Applied Surface Science*, 2009, **255**, 4470-4473.
9. G. Shen, P.-C. Chen, K. Ryu and C. Zhou, *Journal of Materials Chemistry*, 2009, **19**, 828-839.
10. W. Zhu, X. Feng, L. Feng and L. Jiang, *Chemical communications*, 2006, 2753-2755.
11. K. J. Choi and H. W. Jang, *Sensors*, 2010, **10**, 4083-4099.
12. G. Shen and D. Chen, *Frontiers of Optoelectronics in China*, 2010, **3**, 125-138.
13. J. Huang and Q. Wan, *Sensors*, 2009, **9**, 9903-9924.
14. C. Ye, Y. Bando, G. Shen and D. Golberg, *The Journal of Physical Chemistry B*, 2006, **110**, 15146-15151.
15. J. Yu, J. Zhang and S. Liu, *The Journal of Physical Chemistry C*, 2010, **114**, 13642-13649.
16. C. Karunakaran, S. SakthiRaadha, P. Gomathisankar and P. Vinayagamoorthy, *Powder Technology*, 2013, **246**, 635-642.
17. X. Cui, H. Ma, B. Wang and H. Chen, *Journal of hazardous materials*, 2007, **147**, 800-805.
18. J. A. Melero, J. Iglesias and G. Morales, *Green Chem*, 2009, **11**, 1285–1308.
19. T. Tanaka and A. Osuka, *Chemical Society Reviews*, 2015, **44**, 943-969.
20. H. K. Hombrecher, S. Ohm and D. Koll, *Tetrahedron*, 1996, **52**, 5441-5448.
21. S. M. Ló, D. R. Ducatti, M. E. R. Duarte, S. M. Barreira, M. D. Noseda and A. G. Gonçalves, *Tetrahedron Letters*, 2011, **52**, 1441-1443.
22. J. P. Collman, R. Boulatov, C. J. Sunderland and L. Fu, *Chemical reviews*, 2004, **104**, 561-588.
23. X. Ning, L. Ma, S. Zhang, D.-D. Qin, D. Shan, Y. Hu and X.-Q. Lu, *The Journal of Physical Chemistry C*, 2016, **120**, 919–926
24. M. J. Crossley, P. J. Sintic, J. A. Hutchison and K. P. Ghiggino, *Organic & biomolecular chemistry*, 2005, **3**, 852-865.
25. M. Niskanen, M. Kuisma, O. Cramariuc, V. Golovanov, T. I. Hukka, N. Tkachenko and T. T. Rantala, *Physical Chemistry Chemical Physics*, 2013, **15**, 17408-17418.
26. C. Zou, Z. Zhang, X. Xu, Q. Gong, J. Li and C.-D. Wu, *Journal of the American Chemical Society*, 2011, **134**, 87-90.
27. M. P. Byrn, C. J. Curtis, Y. Hsiou, S. I. Khan, P. A. Sawin, S. K. Tendick, A. Terzis and C. E. Strouse, *Journal of the American Chemical Society*, 1993, **115**, 9480-9497.
28. A. M. Shultz, O. K. Farha, J. T. Hupp and S. T. Nguyen, *Journal of the American Chemical Society*, 2009, **131**, 4204-4205.
29. L. Sun, Y. Li, M. Sun, H. Wang, S. Xu, C. Zhang and Q. Yang, *New Journal of Chemistry*, 2011, **35**, 2697-2704.
30. H. Ghafuri, Z.Movahedinia, R. Rahimia and H. R. E. Zand, *RSCAdv.*, **2015**,5, 60172-60178.
31. B. Mandal and B. Basu, *RSC Advances*, 2014, **4**, 13854-13881
32. P. Kumar, G. Singh, D. Tripathi and S. L. Jain, *RSC Advances*, 2014, **4**, 50331-50337
33. S. Rashid, M. Gondal, A. Hameed, M. Aslam, M. Dastageer, Z. Yamani and D. Anjum, *RSC Advances*, 2015, **5**, 32323-32332.
34. Subramaniam. T, Kesavan. G, Valmor. R. M and Nagamony. P,*New J. Chem.*, 2014,**38**, 5480-5490
35. X. Wang and L.Andrews, *J. Phys. Chem. A*, 2005, **109**, 9013–9020.
36. A. G. Maki, F. J. Lovas, *Journal of Molecular Spectroscopy* 1983, **98**, 146-153.
37. X. Wang, L. Andrews, *J. Phys. Chem. A* 2006, **110,** 10035-10045.
38. L. J. Boucher, J. J. Katz *J. Am. Chem. Soc.,* 1967, **89**, 1340–134
39. S. P. Adhikari, H. Dean, Z. D. Hood, R. Peng, K. L. More, I. Ivanov, Z. Wu and A. Lachgar, *RSC Advances*, 2015, **5**, 91094-91102.
40. G.Yao, J.Li, Y.Luo, W.Sun, *J. Mol.Catal* A, 2012, **361-362**, 2935.
41. CH.Wang, J.Li, G.Mele, G.M.Yang, F.X.Zhang, L.Palmisano, G.Vasapollo*, Applied Catalysis B*, 2007, **76**, 218226.
42. L. Gomathi Devi, R. Kavitha, *RSC Adv*, 2014, **4**, 28265

View Article Online
DOI: 10.1039/C6RA17712C

Synthesis and charactrization of a new magnetic nanocomposite with metalloporphyrin (CoTPyP) and sulfated tin dioxide (Fe_3O_4@SnO_2/SO_4^{2-}), and investigation of its photocatalytic effects on degradation of Rhodamine B

Hossein Ghafuri*[a], Fatemeh Mohammadi[a] and Rahmatallah Rahimi[a], Esmaeel Mohammadiyana[a]